



Effect of small changes in sintering temperature on varistor properties and degradation behavior of V–Mn–Nb–Gd co-doped zinc oxide ceramics

C. W. NAHM

Semiconductor Ceramics Laboratory, Department of Electrical Engineering, Dongeui University,
Busan 614-714, Korea

Received 24 May 2014; accepted 8 October 2014

Abstract: The effect of small changes in sintering temperature on microstructure, electrical properties, dielectric characteristics, and degradation behavior of V–Mn–Nb–Gd co-doped zinc oxide ceramics was investigated. With the increase of sintering temperature, the densities of the sintered pellets decreased from 5.54 to 5.42 g/cm³ and the average grain size increased from 4.1 to 11.7 μm. The breakdown field ($E_{1\text{ mA}}$) decreased noticeably from 7138 to 920 V/cm with the increase of sintering temperature. The varistor ceramics sintered at 900 °C exhibited excellent nonohmic properties, which were 66 for the nonohmic coefficient and 77 μA/cm² for the leakage current density. Concerning stability, the varistors sintered at 900 °C exhibited the strongest accelerated degradation characteristics, with $\Delta E_{1\text{ mA}} = -9.2\%$ for DC accelerated degradation stress of $0.85 E_{1\text{ mA}}$ at 85 °C for 24 h.

Key words: ZnO–V₂O₅-based ceramics; sintering; electrical properties; degradation behavior; varistor

1 Introduction

Essentially, semiconductor devices and IT systems are very susceptible or vulnerable to transient overvoltages such as electrostatic discharge (ESD), switching of electrical loads, magnetic and inductive coupling. Transient can originate from inside or outside a facility. However, the majority of surges are created within a facility. This is attributed to electrical circumstance that electronic systems are very complex and dense, because of a number of components and extremely narrow space between electric lines.

ZnO varistor ceramics are well known as a surge protection device (SPD) made by sintering ZnO powder modified with subordinate additives such as CoO, Sb₂O₃, MnO₂, Cr₂O₃, together with Bi₂O₃ (or Pr₆O₁₁) as main additives [1–5]. Electrically, they exhibit symmetric V-I characteristics similar to a back-to-back Zener diode having a single junction [1–3]. Microstructurally, they are featured by multi-junctions composed of grain and grain boundaries, which are distributed three-dimensionally through sintered ceramics.

Commercial multilayered chip varistor (MLV) ceramics are based on Bi₂O₃ and Pr₆O₁₁ as a varistor-

former. ZnO ceramics added with Bi₂O₃ and Pr₆O₁₁ require a high sintering temperature and consequently have no choice but to use a refractory related to Pd or Pt as an inner-electrode. New ZnO ceramics added with V₂O₅ as a varistor-former have an important advantage, which can use much cheaper Ag, when compared with Pd or Pt [6,7]. Until now, a study on ZnO–V₂O₅-based ceramics has been investigated in many points: microstructure, electrical properties, dielectric characteristics, and degradation behavior according to experimental variables such as additives and sintering process [8–18]. However, yet there are many problems to be solved in order to use commercially. The sintering process for specific composition can improve nonohmic properties in the ZnO–V₂O₅ ceramics [11,12,14–18]. Therefore, it is very interesting to investigate how the sintering process affects varistor properties for specific composition. In this work, sintering temperature dependence on microstructure, nonohmic properties, dielectric characteristics, and DC-degradation behavior of the V–Mn–Nb–Gd co-doped zinc oxide ceramics was investigated at low temperatures of 875, 900, 925, and 950 °C, respectively. A surprisingly high nonohmic coefficient and high stability were attained by a proper sintering process.

2 Experimental

High-purity (>99.9%) reagent-grade raw materials composed of 97.35% ZnO (mole fraction, Aldrich Chemical Co., USA), 0.5% V₂O₅ (Kojundo Chemical Laboratory, Japan), 2.0% MnO₂ (Kojundo Chemical Laboratory, Japan), 0.1% Nb₂O₅ (Kojundo Chemical Laboratory, Japan), 0.05% Gd₂O₃ (Kojundo Chemical Laboratory, Japan) were prepared. Raw materials were mixed by ball milling with zirconia balls and acetone in a polypropylene bottle for 24 h. The mixture was dried at 120 °C for 12 h. The dried mixture was put into container with acetone and 0.8% polyvinyl butyral (PVB, mass fraction) binder of powder. After drying, the mixture was granulated by sieving through a screen with a pore diameter of 0.15 mm to produce the starting powder. The sieved powder was pressed into disk-shaped pellets of 10 mm in diameter and 1.5 mm in thickness at a pressure of 100 MPa. The pellets were set on MgO plate and sintered at different temperatures (875, 900, 925 and 950 °C) in air for 3 h, and furnace-cooled to room temperature. The heating and cooling rates were 4 °C/min. The final pellets were roughly 8 mm in diameter and 1.0 mm in thickness. Conductive silver paste was coated by screen-printing techniques on both faces of the pellets and the electrodes were formed by heating it at 550 °C for 10 min. The electrodes were 5 mm in diameter. Finally, after soldering the lead wire to both electrodes, the samples were packaged by dipping them into a thermoplastic resin powder.

One side of the samples was lapped and ground with SiC paper, and then polished with 0.3 μm-Al₂O₃ powder to a mirror-like surface. The polished samples were chemically etched in HClO₄–H₂O solution (1:1000, volume ratio) at 25 °C for 25 s. The surface microstructure was examined by a field emission scanning electron microscope (FESEM, Quanta 200, FEI, Brno, Czech). The average grain size (d) was determined by the linear intercept method [19]. The crystalline phases were identified by X-ray diffractometer (XRD, X'pert-PRO MPD, Panalytical, Almelo, Netherlands) with Cu K_α radiation. The density (ρ) of the sintered pellet was measured using a density determination kit (238490) attached to balance (AG 245, Mettler Toledo International Inc., Greifensee, Switzerland).

The electric field (E)–current density (J) characteristics were measured using a high voltage source-measure unit (Keithley 237, Keithley Instruments Inc., Cleveland, OH, USA). The breakdown field ($E_{1\text{ mA}}$) was measured at a current density of 1.0 mA/cm² and the leakage current density (J_L) was measured at $0.80E_{1\text{ mA}}$. The nonohmic coefficient (α) was determined through the expression, $\alpha = (\lg J_2 - \lg J_1) / (\lg E_2 - \lg E_1)$, where E_1

and E_2 are the electric fields corresponding to $J_1 = 1.0 \text{ mA/cm}^2$ and $J_2 = 10 \text{ mA/cm}^2$, respectively. The dielectric behavior in accordance with frequency for the apparent dielectric constant (ϵ'_{APP}) and dissipation factor ($\tan \delta$) of the samples was measured in the range of 100 Hz–2 MHz using an RLC meter (QuadTech 7600, Marlborough, MA, USA).

The DC-accelerated degradation test was performed for stress state of $0.85E_{1\text{ mA}}$ at 85 °C for 24 h. Simultaneously, the leakage current was monitored at intervals of 1 min during stressing using a high voltage source-measure unit (Keithley 237, Keithley Instruments Inc., Cleveland, OH, USA). The degradation rate coefficient (K_T) was calculated through the expression $I_L = I_{L0} + K_T t^{1/2}$, where I_L is the leakage current at stress time (t) and I_{L0} is I_L at $t=0$ [20]. After application of a stress, the E – J characteristics were measured at room temperature.

3 Results and discussion

Figure 1 shows the SEM micrographs of the samples sintered at different temperatures. Outwardly, firstly a remarkable difference cannot be found when compared with the surface morphologies of other ZnO–V₂O₅-based varistor ceramics, and secondarily the grain size changes greatly despite small changes in the sintering temperature, in particular, exceeding 925 °C. Finally, it can be seen that the pores exist at the grain boundaries. The microstructure characteristic parameters are summarized in Table 1. The average grain size increased remarkably in the range of 4.1–11.7 μm in spite of small sintering changes with the increase of sintering temperature. The density of sintered pellets decreased from 5.54 to 5.42 g/cm³ corresponding to 95.8%–93.8% of the theoretical density (ρ_{TD}) (pure ZnO, $\rho_{\text{TD}} = 5.78 \text{ g/cm}^3$) with the increase of sintering temperature. This is attributed to the volatility of the V-species for V₂O₅ with low melting point as low as 690 °C.

The XRD patterns of the samples at different sintering temperatures are shown in Fig. 2. These patterns revealed the presence of Zn₃(VO₄)₂, ZnV₂O₄, GdVO₄, and VO₂ as minor secondary phases. Among minor phases, ZnV₂O₄ ($2\theta = 30.0789^\circ, 35.4033^\circ$) and VO₂ ($2\theta = 28.0650^\circ$) almost disappeared when the sintering temperature exceeded 925 °C. It is assumed that this is related to the volatility of liquid phase when the sintering temperature exceeds 925 °C. The disappearance of ZnV₂O₄ and VO₂ may affect nonohmic properties. In contrast, no GdVO₄ was affected by sintering temperature.

Figure 3 shows the electric field–current density (E – J) characteristics of the samples sintered at different

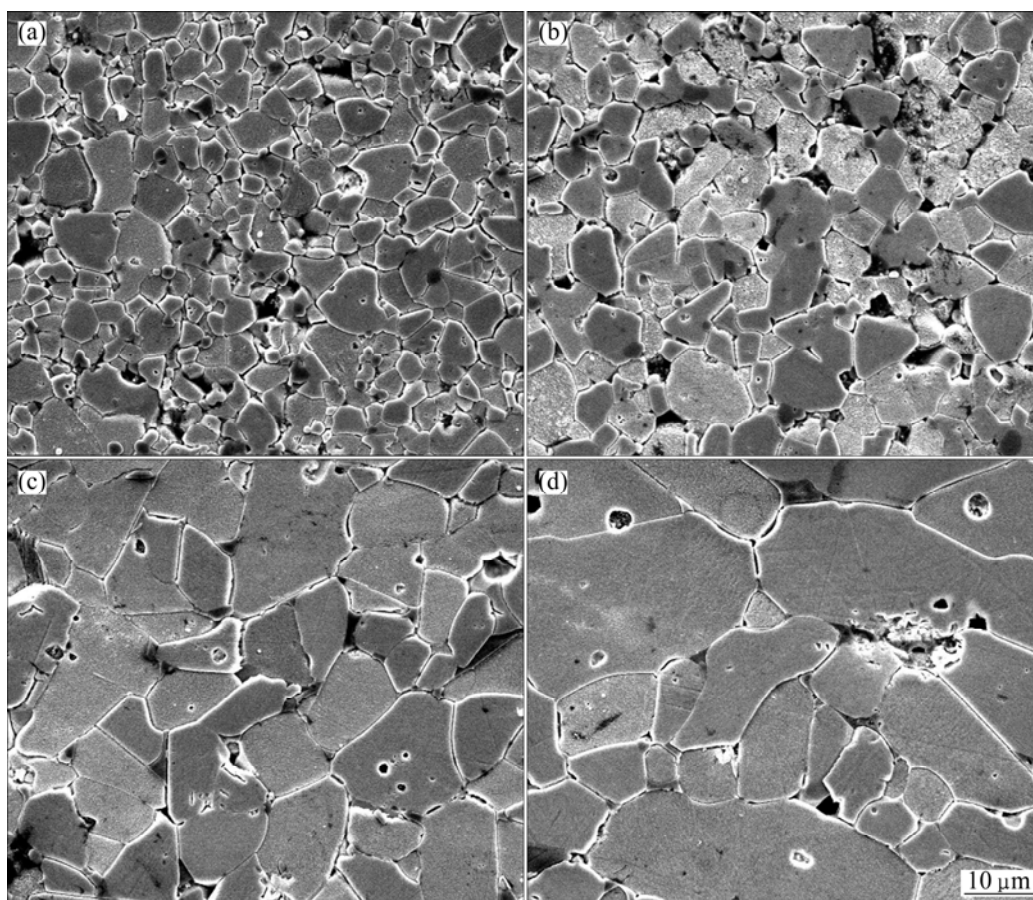


Fig. 1 SEM micrographs of samples sintered at different temperatures: (a) 875 °C; (b) 900 °C; (c) 925 °C; (d) 950 °C

Table 1 Average grain size, sintered density, electrical and dielectric parameters of samples sintered at different temperatures

Sintering temperature/°C	d /μm	ρ /(g·cm ⁻³)	$E_{1\text{ mA}}/$ (V·cm ⁻¹)	V_{gb}/V	α	$J_1/$ (μA·cm ⁻²)	ϵ'_{APP} at 1 kHz	$\tan \delta$ at 1 kHz	$\tan \delta$ at 1 MHz
875	4.1	5.54	7138	2.9	50.9	135.0	394.8	0.273	0.136
900	5.3	5.49	5365	2.8	66.1	77.0	546.5	0.197	0.152
925	8.1	5.47	3024	2.4	26.6	270.1	899.9	0.349	0.137
950	11.7	5.42	920	1.1	19.0	119.4	3347.0	0.212	0.255

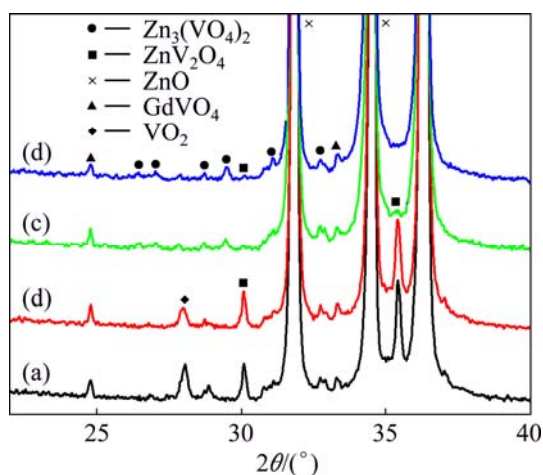


Fig. 2 XRD patterns of samples sintered at different temperatures: (a) 875 °C; (b) 900 °C; (c) 925 °C; (d) 950 °C

temperatures. The varistor properties are featured by the nonohmicity in the E – J relation. The characteristic curves are composed of two states: one is current-off state before breakdown field, the other is current-on state after breakdown field. However, the shape of edge between ohmic region and nonohmic region shows an obvious difference with sintering temperature. The E – J characteristic parameters obtained from E – J curves are summarized in Table 1.

Figure 4 shows grain size, sintered density and electrical and dielectric parameters of the samples sintered at different temperatures. The behavior of breakdown field ($E_{1\text{ mA}}$) as a function of sintering temperature is indicated graphically in Fig. 4(c). The $E_{1\text{ mA}}$ decreased abruptly from 7138 to 920 V/cm despite small sintering changes with the increase of sintering

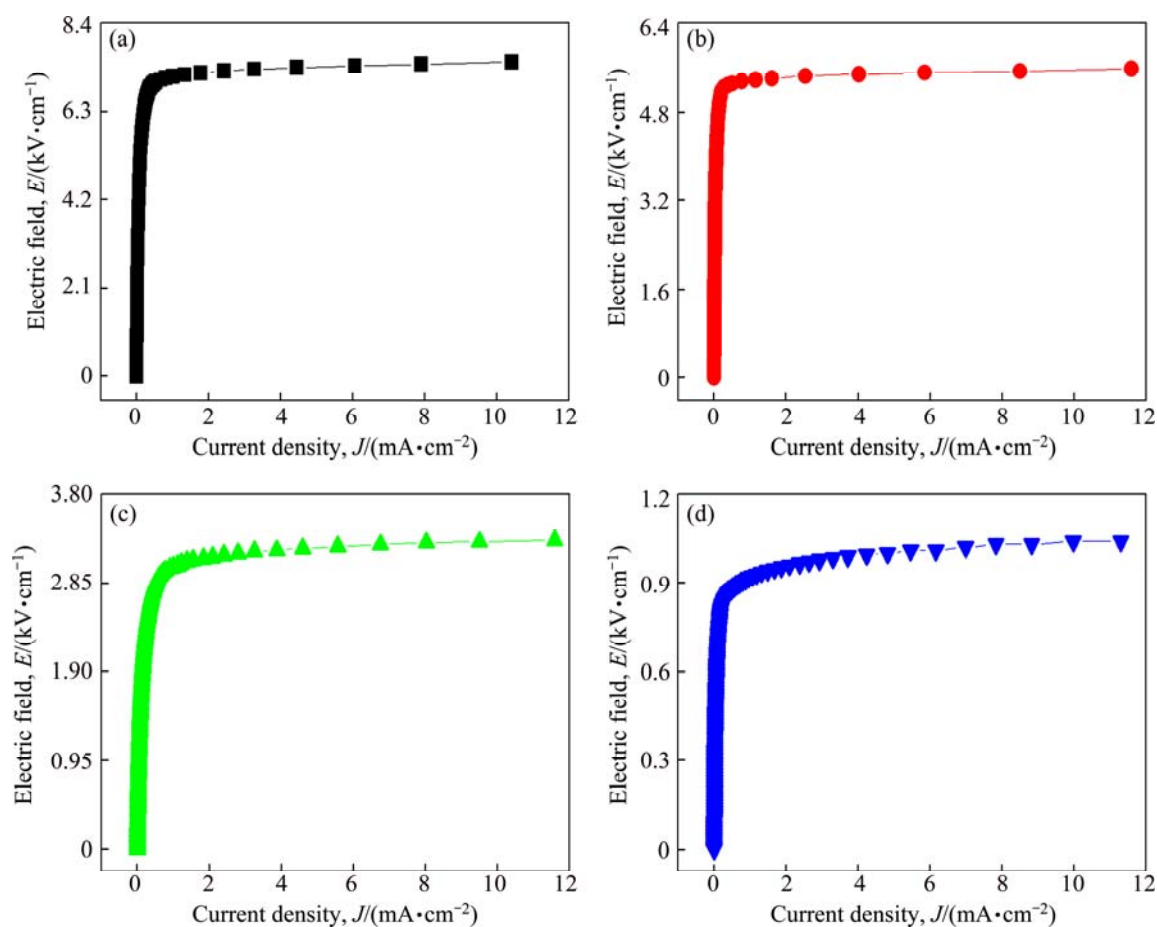


Fig. 3 E - J characteristics of samples sintered at different temperatures: (a) 875 °C; (b) 900 °C; (c) 925 °C; (d) 950 °C

temperature. The $E_{1\text{ mA}}$ is predominantly controlled by the grain size (d), and slightly depends on the breakdown voltage per grain boundaries (V_{gb}). The breakdown voltage (V_{B}) is indicated as: $V_{\text{B}} = (D/d)V_{\text{gb}} = nV_{\text{gb}}$, furthermore, $E_{1\text{ mA}}$ is written as $E_{1\text{ mA}} = V_{\text{gb}}/d$, where D is the thickness of sample, and n is the number of grain boundaries [1,3]. Therefore, V_{B} is proportional to n and V_{gb} . In general, to control the breakdown voltage, one is to control the sample thickness at the fixed grain size, the other is to control the grain size at the constant sample thickness. As a result, the decrease of $E_{1\text{ mA}}$ with the increase of sintering temperature is attributed to the increase of the average ZnO grain size and the decrease of breakdown voltage per grain boundary.

The behavior of nonohmic coefficient (α) as a function of sintering temperature is indicated graphically in Fig. 4(d). The α value increased from 51 to 66 when the sintering temperature was increased from 875 to 900 °C and then decreased to 19 when the sintering temperature was further increased from 900 to 950 °C. In the light of changing tendency, it can be seen that the sintering temperature in this system has a strong effect on nonohmic properties in spite of small sintering changes. It should be emphasized that the sample sintered at a temperature as low as 900 °C exhibited the

highest value ($\alpha=66$), when compared with other varistors reported until now [15–17]. In addition, it is worth noting that the sample sintered at a temperature as low as 875 °C exhibited a high α value, reaching $\alpha=51$. However, α value abruptly decreased less than 30 when the sintering temperature exceeded 925 °C. The behavior of α with sintering temperature is related to the potential barrier height, which strongly depends on the electronic trap states, such as the zinc vacancies, interstitial zinc, ionized donor-like and oxygen at the grain boundaries. Furthermore, these defects will vary the density of interface states at the grain boundaries. Based on XRD analysis, it is assumed that the disappearance of ZnV_2O_4 and VO_2 will change the density of interface states when the sintering temperature exceeds 925 °C, in the light of the decrease of nonohmic coefficient.

The behavior of leakage current density (J_{L}) as a function of sintering temperature is indicated graphically in Fig. 4(e). The J_{L} value decreased from 135 to 77 $\mu\text{A}/\text{cm}^2$ with the increase of sintering temperature up to 900 °C. Thereafter it increased up to 925 °C and again decreased up to 950 °C. Therefore, it was found to have a fluctuation with the increase of sintering temperature.

Figure 5 shows the apparent dielectric constant ($\varepsilon'_{\text{APP}}$) and dissipation factor ($\tan \delta$) of the samples

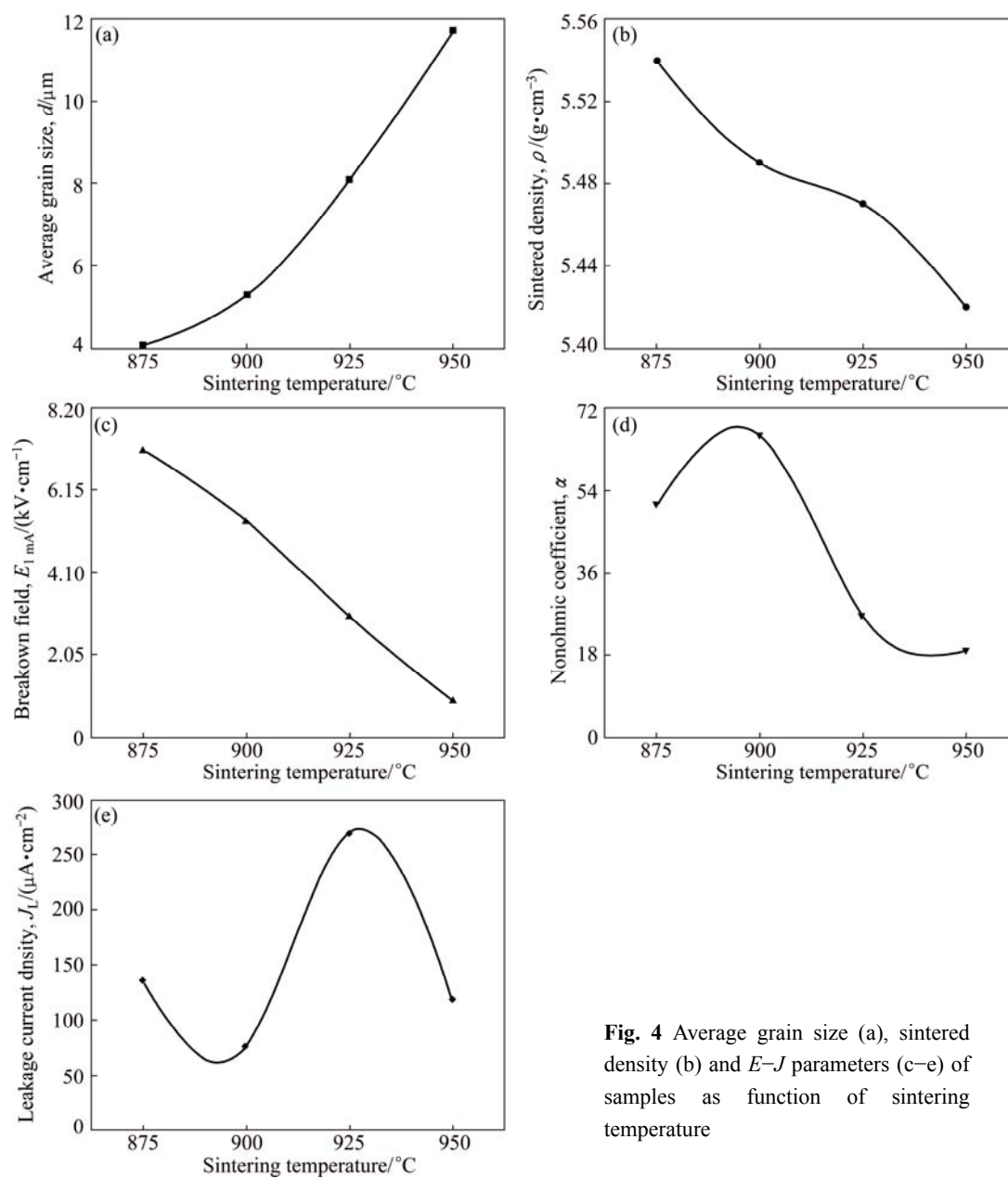


Fig. 4 Average grain size (a), sintered density (b) and E - J parameters (c-e) of samples as function of sintering temperature

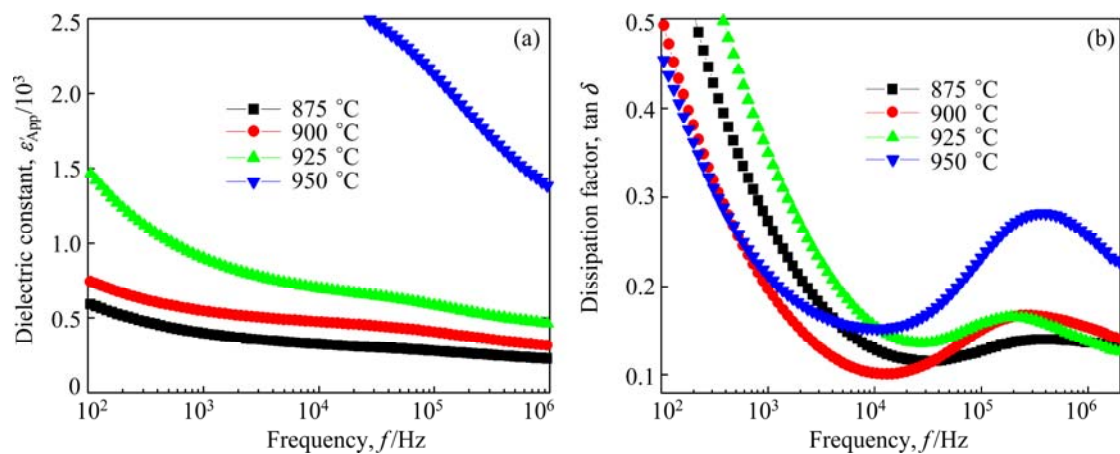


Fig. 5 Dielectric characteristics of samples vs frequency at different sintering temperatures: (a) Dielectric constant, ϵ'_{APP} ; (b) Dissipation factor, $\tan \delta$

sintered at different temperatures. The behavior of $\varepsilon'_{\text{APP}}$ for all samples showed the dielectric dispersion phenomena, which decreased with an increase in the frequency. The decrease of $\varepsilon'_{\text{APP}}$ with increasing frequency is attributed to the decrease of the number of dipole, which can follow to test frequency. In particular, the dielectric dispersion for all samples in common was large at below 1 kHz and above 100 kHz. In addition, the dielectric dispersion increased with the increase of sintering temperature. The $\varepsilon'_{\text{APP}}$ increased with the increase of sintering temperature in the range of overall frequency. On the other hand, $\tan \delta$ decreased abruptly until the vicinity of roughly 10 kHz with increasing frequency and exhibited a dielectric absorption peak in the vicinity of 200–300 kHz, and thereafter again decreased. The detailed dielectric characteristic parameters are summarized in Table 1.

The behavior of $\varepsilon'_{\text{APP}}$ at 1 kHz as a function of sintering temperature is indicated graphically in Fig. 6(a). The $\varepsilon'_{\text{APP}}$ increased from 394.8 to 3347.0 with the increase of sintering temperature from 875 to 950 °C. This is directly related to the average grain size and depletion layer width, as can be seen in the following expression: $\varepsilon'_{\text{APP}} = \varepsilon_g(d/t)$, where ε_g is the dielectric

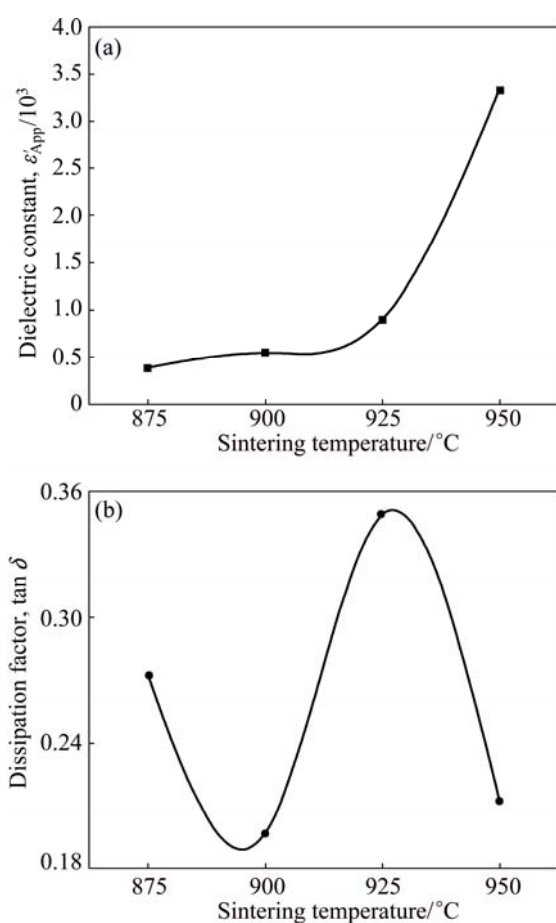


Fig. 6 Dielectric parameters as function of sintering temperature: (a) Dielectric constant, $\varepsilon'_{\text{APP}}$; (b) Dissipation factor, $\tan \delta$

constant of ZnO (8.5), d is the average grain size, and t is the depletion layer width of the both sides at the grain boundaries. The behavior of $\tan \delta$ at 1 kHz as a function of sintering temperature is indicated graphically in Fig. 6(b). The $\tan \delta$ at 1 kHz was found to have a fluctuation with the increase of sintering temperature. The sample sintered at 900 °C exhibited the lowest value (0.197) in the $\tan \delta$ at 1 kHz. On the whole, the changing tendency of $\tan \delta$ was similar to that of leakage current in accordance with sintering temperature. However, the behavior of $\tan \delta$ at 1 MHz is entirely different from that at 1 kHz. At present, it is assumed that this is attributed to the dipolar rotation with frequency.

Figure 7 shows the behavior of leakage current (I_L) during DC accelerated degradation stress of $0.85 E_{1\text{mA}}$ at 85 °C for 24 h for the samples sintered at different temperatures. Obviously, it can be seen that the sintering temperature has a noticeable effect on the behavior of I_L for applying the stress. The sample sintered at 875 °C exhibited the thermal runaway in a few seconds for applying the stress. In general, the density of the sintered pellet and the leakage current greatly have a significant effect on the stability. The low sintered density decreased the number of conduction path and eventually led to the concentration of current. The high leakage current led to repetition cycle between joule heating and leakage current. Although the samples sintered at 875 °C exhibited relatively high sintered density, they seemed to exhibit extremely low stability due to much higher leakage current. The sample sintered at 925 °C exhibited a positive creep of leakage current (PCLC), in which the I_L abruptly increased with the increase of the stress time. The stability of the samples can be estimated by the degradation rate coefficient (K_T), indicating the degree of degradation. This is the slope of leakage current for the stress time and lower K_T leads to higher stability. As a result, the K_T value of the samples sintered at 925 °C was

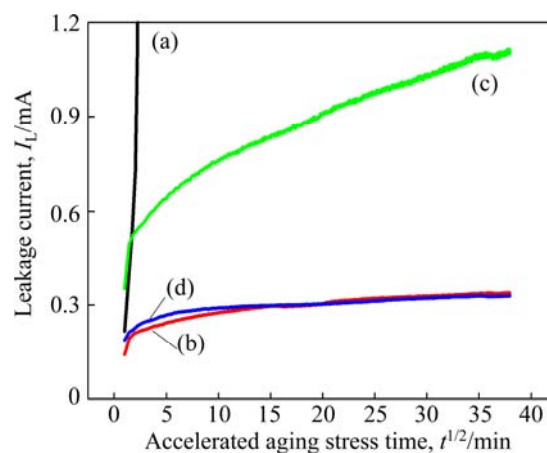


Fig. 7 Leakage current behavior during stress of samples sintered at different temperatures: (a) 875 °C; (b) 900 °C; (c) 925 °C; (d) 950 °C

$103.2 \mu\text{A}\cdot\text{h}^{-1/2}$. In contrast, the samples sintered at 900 and 950 °C exhibited weak PCLC, in which I_L gradually increased with the increase of the stress time. They showed a good stability, which exhibited 19.6 and $13.3 \mu\text{A}\cdot\text{h}^{-1/2}$ in K_T , respectively. The behavior of I_L with the stress in these samples is obviously different from that of Zn–V–Mn–Nb (ZVMN) varistors modified with Er_2O_3 and Bi_2O_3 [16,17].

Figure 8 shows the effect of sintering temperature of E – J characteristics before and after application of a stress of the samples sintered at different temperatures. It can be seen that the sintering temperature has a significant effect on E – J curves after application of a stress. The sample sintered at 875 °C exhibited a large variation in the E – J characteristics because of thermal runaway after application of a stress. This sample lost almost nonohmic properties. Next, the sample sintered at 925 °C exhibited a large difference, when compared with initial E – J characteristics curve. Also this sample showed a weak stability against the stress. The sample sintered at 950 °C exhibited a significant variation in the vicinity of the knee. The sample sintered at 900 °C exhibited the smallest variation of E – J characteristics, when compared with other samples after application of a stress. However, this sample also accompanied small

variation in the vicinity of knee. The variations of E – J characteristic parameters before and after application of a stress of the samples sintered at different temperatures are summarized in Table 2. The behavior of $E_{1\text{ mA}}$ and α after application of a stress with initial $E_{1\text{ mA}}$ and α for the samples sintered at different temperatures is indicated graphically in Fig. 9. The variation rate in $E_{1\text{ mA}}$ after application of a stress increased in the order of 900→950→925→950 °C. Only the sample sintered at 900 °C exhibited the $\Delta E_{1\text{ mA}}$ less than 10% after application of a stress. On the other hand, α after applying the stress greatly changed unlike $E_{1\text{ mA}}$. All samples except for the sample sintered at 900 °C decreased considerably less than 10 in the nonohmic coefficient after application of a stress. However, the sample sintered at 900 °C exhibited the nonohmic coefficient more than 20 after applying the stress. On the whole, also, the J_L value increased extremely after application of a stress unlike $E_{1\text{ mA}}$ and α .

4 Conclusions

The microstructure, electrical properties, dielectric characteristics, and degradation behavior of V–Mn–Nb–Gd co-doped zinc oxide ceramics were systematically

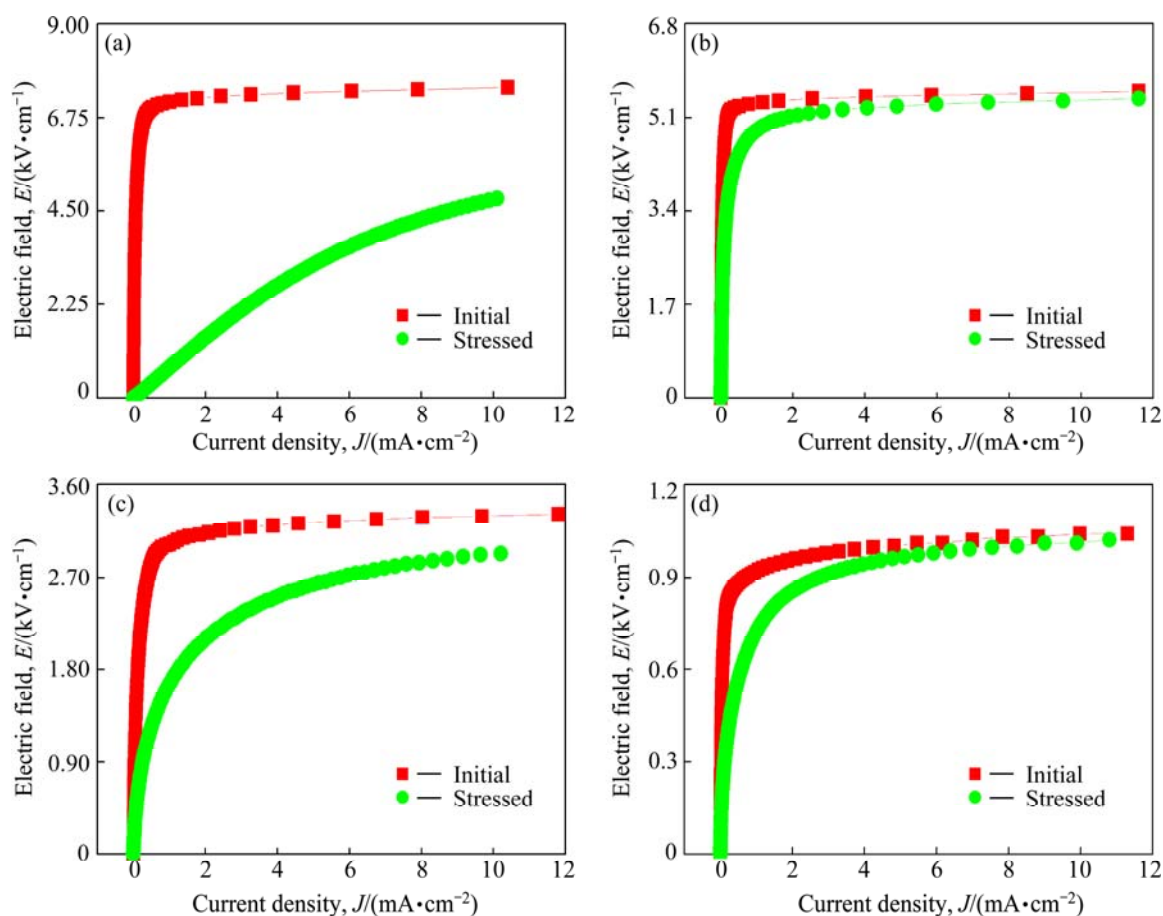
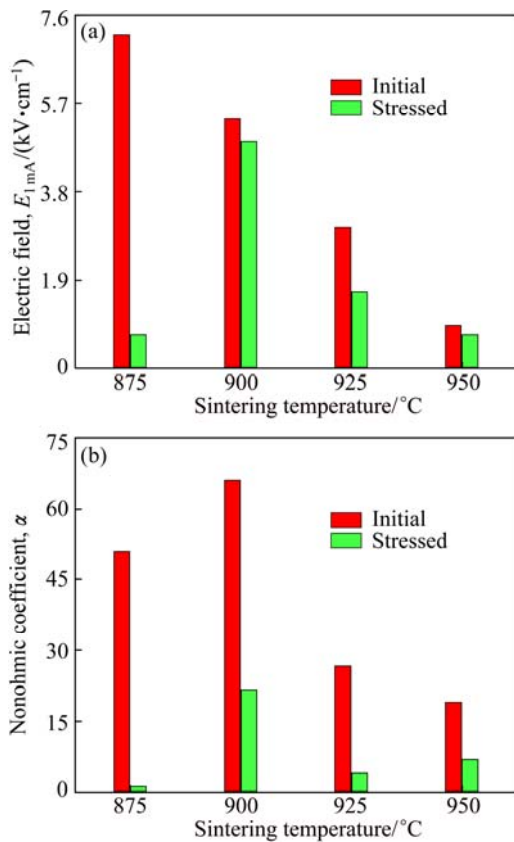


Fig. 8 E – J characteristic behavior before and after application of stress of samples sintered at different temperatures: (a) 875 °C; (b) 900 °C; (c) 925 °C; (d) 950 °C

Table 2 E - J characteristic parameters of samples sintered at different temperatures before and after application of stress

Sintering temperature/ °C	Stress state	$K_T/$ ($\mu\text{A}\cdot\text{h}^{-1/2}$)	$E_{1\text{mA}}/$ ($\text{V}\cdot\text{cm}^{-1}$)	$\Delta E_{1\text{mA}}/\%$	α	$\Delta\alpha/\%$	$J_L/$ ($\mu\text{A}\cdot\text{cm}^{-2}$)	$\Delta J_L/\%$
875	Initial	—	7138	—	51	—	135.0	—
	Stressed	Thermal runaway						
900	Initial	—	5365	—	66	—	77.0	—
	Stressed	19.6	4870	−9.2	22	−66.7	264.6	243.6
925	Initial	—	3024	—	27	—	270.1	—
	Stressed	103.2	1656	−45.2	4	−85.2	579.8	114.7
950	Initial	—	920	—	19	—	119.4	—
	Stressed	13.3	723	−21.4	7	−63.1	526.4	340.5

**Fig. 9** E - J characteristic parameters before and after application of stress of samples sintered at different temperatures: (a) Breakdown field $E_{1\text{mA}}$; (b) Nonohmic coefficient α

investigated for the samples sintered at different temperatures. Increasing sintering temperature yielded the decrease in the sintered density and the increase in the average grain size. The breakdown field decreased with the increase of sintering temperature. The varistor ceramics sintered at 900 °C exhibited excellent nonohmic properties, with a high nonohmic coefficient ($\alpha=66$). Furthermore, the varistor ceramics sintered at 900 °C exhibited the highest stability, with $\Delta E_{1\text{mA}} = -9.2\%$ for DC accelerated degradation stress of $0.85E_{1\text{mA}}$ at 85 °C for 24 h.

References

- [1] LEVINSON L M, PILIPP H R. Zinc oxide varistor—A review [J]. American Ceramic Society Bulletin, 1986, 65: 639–646.
- [2] MUKAE K. Zinc oxide varistors with praseodymium oxide [J]. American Ceramic Society Bulletin, 1987, 66: 1329–1331.
- [3] GUPTA T K. Application of zinc oxide varistor [J]. Journal of the American Ceramic Society, 1990, 73: 1817–1840.
- [4] CHEN G H, LI J L, YANG Y, YUAN C L, ZHOU C R. Microstructure and electrical properties of Dy₂O₃-doped ZnO–Bi₂O₃ based varistor ceramics [J]. Materials Research Bulletin, 2014, 50: 141–147.
- [5] NAHM C W. The nonlinear properties and stability of ZnO–Pr₆O₁₁–CoO–Cr₂O₃–Er₂O₃ ceramic varistors [J]. Materials Letters, 2001, 47: 182–187.
- [6] TSAI J K, WU T B. Non-ohmic characteristics of ZnO–V₂O₅ ceramics [J]. Journal of Applied Physics, 1994, 76: 4817–4822.
- [7] TSAI J K, WU T B. Microstructure and nonohmic properties of binary ZnO–V₂O₅ ceramics sintered at 900 °C [J]. Materials Letters, 1996, 26: 199–203.
- [8] HNG H H, KNOWLES K M. Knowles, microstructure and current-voltage characteristics of multicomponent vanadium-doped zinc oxide varistors [J]. Journal of the American Ceramic Society, 2000, 83: 2455–2462.
- [9] HNG H H, CHAN P L. Effects of MnO₂ doping in V₂O₅-doped ZnO varistor system [J]. Materials Chemistry Physics, 2002, 75: 61–66.
- [10] CHEN C S. Effect of dopant valence state of Mn-ions on the microstructures and nonlinear properties of microwave sintered ZnO–V₂O₅ varistors [J]. Journal of Materials Science, 2003, 38: 1033–1038.
- [11] NAHM C W. DC accelerated aging behavior of Co–Dy–Nb doped Zn–V–M-based varistors with sintering process [J]. Journal of Materials Science: Materials in Electronics, 2011, 22: 444–451.
- [12] NAHM C W. Sintering effect on pulse aging behavior of Zn–V–Mn–Co–Dy–Nb varistors [J]. Journal of the American Ceramic Society, 2011, 94: 2269–2272.
- [13] MING Z, YU S, SHENG T C. Grain growth of ZnO–V₂O₅ based varistor ceramics with different antimony dopants [J]. Journal of the European Ceramic Society, 2011, 31: 2331–2337.
- [14] NAHM C W. Effect of sintering process on electrical properties and ageing behavior of ZnO–V₂O₅–MnO₂–Nb₂O₅ varistor ceramics [J]. Journal of Materials Science: Materials in Electronics, 2012, 23: 457–463.
- [15] NAHM C W. Major effects on electrical properties of ZnO–V₂O₅–MnO₂–Nb₂O₅–Er₂O₃ ceramics with sintering changes [J]. Ceramics International, 2012, 38: 2593–2596.

- [16] NAHM C W. Effect of sintering temperature on electrical properties, dielectric characteristics, and aging behavior of ZnO–V₂O₅-based varistor ceramics modified with Bi₂O₃ [J]. Journal of Materials Science: Materials in Electronics, 2013, 24: 118–124.
- [17] NAHM C W. Improvement of aging characteristics of (Mn, Nb, Er)-doped ZnO–V₂O₅-based varistor ceramics by small sintering changes [J]. Journal of Materials Science: Materials in Electronics, 2013, 24: 2228–2233.
- [18] MIRZAYI M, HEKMATSHOAR M H. Effect of V₂O₅ on electrical and microstructural properties of ZnO ceramics [J]. Physica B, 2013, 414: 50–55.
- [19] WURST J C, NELSON J A. Lineal intercept technique for measuring grain size in two-phase polycrystalline ceramics [J]. Journal of the American Ceramic Society, 1972, 55: 109–111.
- [20] FAN J, FREER R. Deep level transient spectroscopy of zinc oxide varistors doped with aluminum oxide and/or silver oxide [J]. Journal of the American Ceramic Society, 1994, 77: 2663–2668.

烧结温度的细微变化对 V–Mn–Nb–Gd 共掺杂氧化锌陶瓷压敏特性和衰减行为的影响

C. W. NAHM

Semiconductor Ceramics Laboratory, Department of Electrical Engineering, Donggeui University,
Busan 614-714, Korea

摘 要: 研究烧结温度的细微变化对 V–Mn–Nb–Gd 共掺杂氧化锌陶瓷显微组织、电性能、介电性能和衰减行为的影响。随着烧结温度的升高, 烧结球团密度由 5.54 g/cm³ 降低到 5.42 g/cm³, 平均晶粒尺寸由 4.1 μm 增大至 11.7 μm, 击穿场强由 7138 V/cm 急剧降低至 920 V/cm。在 900 °C 烧结的压敏陶瓷呈现极佳的非线性(非欧姆)特性, 其非线性系数和漏电流密度分别为 66 和 77 μA/cm²。在性能稳定性方面, 在 85 °C、24 h 和 0.85E_{1 mA} 的直流加速应力下, 经 900 °C 烧结的压敏陶瓷呈现最强的加速衰减特性, 且其 ΔE_{1 mA}=–9.2%。

关键词: ZnO–V₂O₅ 基陶瓷; 烧结; 电性能; 衰减行为; 压敏电阻器

(Edited by Wei-ping CHEN)